PNAS RESEARCH ARTICLE | PHYSICS

Superradiant Thomson scattering from graphite in the extreme ultraviolet

Claudia Fasolato[a,b,1], Elena Stellino[a], Emiliano Principi[c], Riccardo Mincigrucci[c], Jacopo Stefano Pelli-Cresi[c], Laura Foglia[c], Paolo Postorino[d], Francesco Sacchetti[a,e], and Caterina Petrillo[a,f]

Edited by Siegfried H. Glenzer, SLAC National Accelerator Laboratory, Menlo Park, CA; received December 16, 2022; accepted December 5, 2023 by Editorial Board Member Bernard F. Schutz

We study the Thomson scattering from highly oriented pyrolitic graphite excited by the extreme ultraviolet, coherent pulses of FERMI free electron laser (FEL). An apparent nonlinear behavior is observed and fully described in terms of the coherent nature of both exciting FEL beam and scattered radiation, producing an intensity-dependent enhancement of the Thomson scattering cross-section. The process resembles Dicke's superradiant phenomenon and is thus interpreted as the observation of superradiant Thomson scattering. The process also triggers the creation of coherent, low-q (< 0.3 Å^{-1}), low energy phonons. The experimental data and analysis provide quantitative information on the sample characteristics, absorption, scattering factor, and coherent phonon energies and populations and open the route for the investigation of the deep nature of complex materials.

superradiant scattering | X-ray phonon scattering | free electron laser

Radiation–matter interaction can be generally described using low-order perturbation theory, due to the relatively small coupling constant $\alpha = e^2/\hbar c \simeq 1/137$ (1, 2). That approximation is considered accurate, in the non-relativistic range, when the incident and scattered radiation can be represented as singly occupied photon states. That condition breaks down in exotic environments, e.g., high energy density astrophysical objects, like pulsars (3, 4), where the radiation states take the form of coherent states with large (>1) average occupation numbers. A (Compton) scattering theory involving coherent radiation states has been long available (5), but specific applications to laboratory scattering experiments do not exist yet. In the last decades, free electron lasers (FELs) opened new routes to study different states of matter (6–8), extending Thomson scattering at short wavelengths (0.05 to 0.2 nm) to the study of low Z elements out of equilibrium (9–13) and providing direct access to the evolution of low energy, coherent excitations in matter in the pump–probe scheme (14–19).

Here, we exploit the high degree of coherence, ensured by the seeded nature of the FEL at FERMI facility (Trieste, Italy), and its high power density ($\approx$ TW/cm^2) in a small space-time range ($\lesssim 10^{-6}$ cm^2 $\times$ 10^2 fs) (19, 20), to explore the nonlinearities in radiation–matter interaction by a properly designed scattering experiment, where coherence in quantum mechanics (QM) plays a crucial role. Over the last decade, the linear response approximation was observed to break down already in transmission experiments, employing intense and short ($<$ 100 fs) extreme ultraviolet (EUV) pulses (21–23). There, the nonlinearity observed was ascribed to the abrupt FEL-induced modification of the sample state, not fundamentally affecting the probe-sample coupling. Instead, in our experiment, we observe a nonlinear amplification of the scattering cross-section which is intrinsic, i.e., not primarily associated with a FEL-modified sample state.

In detail, we observe a positive exponential dependence of the scattered intensity on the incident intensity, varying due to the intrinsic FEL emission fluctuations, and the excitation of low-energy coherent phonons in the material. That effect can be thought as belonging to the class of superradiant processes, defined by Gross and Haroche as "cooperative process(es) involving in a collective mode all the atoms of the sample" (24), leading to an enhanced production of photons with characteristic features. Here, the collective mode is a specific phonon, which couples to the incoming and outgoing photons of the scattering event. Superradiance has been initially predicted (25) and observed (26) in emission experiments, while superradiant scattering has been reported only in astrophysical contexts or analogues (27) and, at the laboratory scale, in the study of the collective excitation of cold atom condensates (28, 29). Here, we present a QM description of a superradiant scattering process from a crystal, in which phonons act as triggered collective modes.

Significance

We present a Thomson scattering study on graphite, excited using the extreme ultraviolet (EUV) pulses (70 fs) of FERMI free electron laser in non-standard experimental conditions, for exciting photon densities and wavelength range. We observe and describe the growth of Thomson cross-section associated with the effect of quantum coherence, in line with Dicke's theory of superradiance, interpreting our observation as a Thomson superradiant scattering process. We believe this work opens the way for a deeper understanding EUV-to-X ray experiments, conducted under the extreme excitation conditions common to the frontier research at free electron lasers. It also provides fundamental insights into linear and nonlinear properties of matter excited in the EUV.

Author contributions: C.F., P.P., F.S., and C.P. designed research; C.F., E.S., E.P., R.M., J.S.P.-C., L.F., F.S., and C.P. performed research; E.P. and R.M. constructed experimental setup; C.F., E.S., and F.S. analyzed data; and C.F., E.S., P.P., F.S., and C.P. wrote the paper.

The authors declare no competing interest.

This article is a PNAS Direct Submission. S.H.G. is a guest editor invited by the Editorial Board.

[1]To whom correspondence may be addressed. Email: claudia.fasolato@cnr.it.

This article contains supporting information online at https://www.pnas.org/lookup/suppl/doi:10.1073/pnas.2221293121/-/DCSupplemental.

Published January 19, 2024.

In scattering processes, the presence of a coherent state of incoming radiation has no specific effect on the probe-sample coupling (5), while a coherent final state produces an amplification of the scattering cross-section at the lowest order of the perturbation theory. That kind of phenomenon is hardly visible in the scattering by electrons in condensed matter physics, where the final states are limited by conservation rules only, while they are more likely observed in phonon scattering, owing to the upper bound of phonon energy, limiting the number of available scattering channels. Hence, a sub-picosecond duration of the FEL probe pulse much shorter than the typical phonon lifetimes (30), yet much longer than the radiation period $\lambda_0/c \approx 0.01$ fs can trigger a coherent scattering process with a final coherent photon state in the Glauber's sense (31), resulting in the observation of a fundamentally nonlinear process. Thus, we found that superradiant scattering experiments in condensed matter allow for exploring the scattering from phonons with final coherent radiation states.

That regime is achievable by employing EUV photons (20) so that only a small fraction of the Brillouin zone (BZ) (i.e., few modes) is accessible and the nonlinear process is activated. Conveniently, in stacked 2D systems, along the unique axis, a reduced number of states in the q—space is sampled, and the number of scattering channels is smaller: Here, the hexagonal graphite is studied as a prototype for 2D systems. That class includes many complex and interesting materials like, for instance, the vast group of transition metal dichalcogenides (32). We will discuss how the described superradiant scattering process triggers nonthermal populations of coherent phonons at low-momentum q in such systems by employing sub-picosecond coherent EUV pulses.

Experimental Design

We carried out a Thomson scattering study on highly oriented pyrolytic graphite (HOPG) using the ≈70 fs EUV pulses of FERMI (33), beamline EIS-TIMEX (16). Two harmonics of FEL-2 configuration were employed, $\lambda_0^{(1)} = 4.08$ nm and $\lambda_0^{(2)} = 4.74$ nm, which correspond to photon energies $\simeq \pm 20$ eV around the carbon absorption K-edge ($E_K \approx 285$ eV) (34). Such wavelengths allow to access the previously unexplored region of low q transfer (8, 9). The sample orientation was fixed (to keep the scattering volume constant), the HOPG c-axis forming a 65° angle with the incident beam, while the angle of detection was varied in the $\theta = 60°$ to 150° range. The sample thickness is about 1 mm; thus, the HOPG can be considered as a bulk system in the present experiment as, considering the absorption properties of the sample, surface effects account for less than 3% of the observed scattering process. The scattering geometry is sketched in Fig. 1*A*. Two FEL linear polarizations (ϵ_0, s and p, perpendicular or parallel to the scattering plane) were used for both λ_0. The incident intensity I_0 was determined, pulse by pulse, by the photocurrent from the FEL focusing mirror, and a microchannel plate (MCP) detector measured the scattered intensity I_{scat}. The energy density was about 0.2 J/cm^2 with 1 μJ pulse. In the worst case ($\lambda_0^{(1)}$), given an absorption length of about 100 nm and the 300-eV photon energy, there is an energy release of about 0.3 eV/atom per pulse: only the accumulation of hundreds of FEL pulses could produce damage, as was directly observed. Accordingly, on each sample spot, a total of five single-shot acquisitions were collected to guarantee the minimum sample damage, by making a pulse-by-pulse statistical control and then shifting the sample by 100 μm to perform a new measurement on a pristine area. In these conditions, only the occupation number of a few, specific vibrational modes is expected to change due to the scattering event.

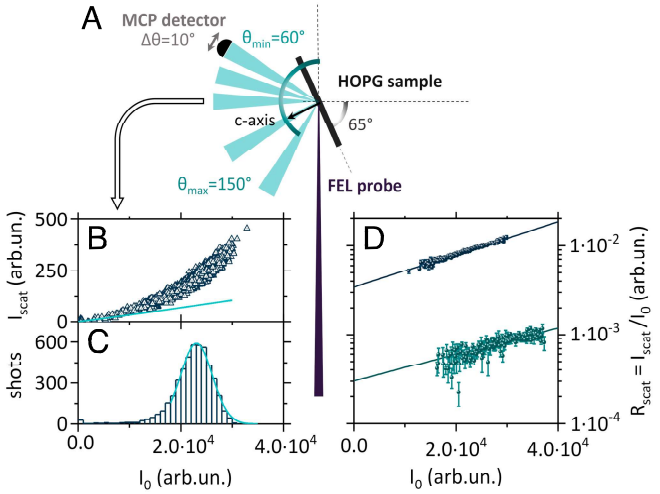

Fig. 1. (*A*) Experimental setup (*Top* view). The FEL beam impinges on the sample tilted by 65°. The scattered radiation is collected by the MCP, with a 10° angular opening, at variable θ (60° to 150°). (*B*) Measured scattered intensity I_{scat} vs. FEL incident intensity I_0 per single shot, for $\lambda_0^{(1)} = 4.08$ nm, ϵ_0 = s, $\theta = 90°$. The linear plot is the trend expected assuming the cross-section as extrapolated ($I_0 \to 0$) from the fitting in panel *D* (see *SI Appendix*, Page S3, for further details). (*C*) I_0 histogram of data in panel (*B*) with Gaussian fitting (see text). (*D*) R_{scat} vs. I_0 for $\lambda_0^{(1)}$ (blue dots) and $\lambda_0^{(2)}$ (cyan dots), ϵ_0 = s, $\theta = 90°$, plotted in a semi-log scale for better visualization. Notice the similar exponential relative increase and the remarkably different value at $I_0 = 0$. Data are corrected according to the statistical analysis (see text). Solid lines are single exponential fits to the data.

Results and Discussion

Thomson Scattering Data: Pretreatment and Observations. Owing to the intrinsic fluctuations of the FEL (35) lasing process (see a histogram of the incident intensity I_0 in Fig. 1*C*), each independent dataset at given $\lambda_0, \epsilon_0, \theta$ of our experiment (Fig. 1*B*) was treated by averaging the ratio of I_{scat} to the incoming I_0, $R_{scat}(I_0) = I_{scat}(I_0)/I_0$, over several different sample points. The average was taken in small enough intervals of I_0. Statistically meaningful data were obtained rejecting the I_0 intervals with too few (<5) data within them and (rare) fluctuations larger than twice the SDs.

In linear Thomson scattering, $R_{scat}(I_0)$ does not depend on I_0 resulting as an intrinsic system property, proportional to the scattering cross-section $\Sigma(\lambda_0, \epsilon_0, \theta) = \int d^2\sigma(\lambda_0, \epsilon_0, \theta)/d\Omega dE$, integrating over final energy and detector solid angle and summing the final polarizations. The observed $R_{scat}(I_0)$ vs. I_0, shown in Fig. 1*D*, appears far from a constant. That happens for every λ_0, ϵ_0. We ruled out the possible experimental artifacts: a saturation of I_0 is not expected, and the low scattered intensity does not support a nonlinear trend of the MCP detector. Furthermore, both I_0 and I_{scat} show Gaussian-like fluctuation distributions (see e.g., the fit to the part of the distribution in Fig. 1*C* considered statistically adequate for the R_{scat} calculation and consequent analysis), thus supporting the absence of undesired anomalies. For additional details on the measurement of intensity, please refer to *SI Appendix*.

Physical Model of the Scattering Cross-Section. To derive useful information from the experiment, we need a model of the

Thomson cross-section in the present conditions. As it is well known, Thomson scattering originates from the coupling between electrons and the radiation field, with both electronic states and nuclear vibrations contributing (14). Thus, the final energy-integrated cross-section is the sum of the electronic $d\sigma/d\Omega|_e$ and the phononic $d\sigma/d\Omega|_{ph}$ contributions. At the first perturbative order, the cross-section is factorized into two terms: a structure factor, containing α^2 and the effect of the system structure, and the sum of the correlation functions describing the electron and phonon dynamics (1, 2).

In the present context, initial and final radiation fields are properly described using coherent states (31) $|I\rangle$ and $|F\rangle$, where all the occupation numbers contribute with Poisson statistics (5), instead of the photon states in the Fock space, with zero or one occupation numbers. Accordingly, one can calculate the transition matrix element $\mathcal{M}_{I,F} \propto \sum_{il} \left\langle F|e^{-i(\boldsymbol{k}-\boldsymbol{k}_0)\cdot(\boldsymbol{r}_i+\boldsymbol{u}_l)}|I\right\rangle$, where $\boldsymbol{r}_i$ and $\boldsymbol{u}_l$ are the electron position and nucleus displacement operators, and $\boldsymbol{k}_0$, $\boldsymbol{k}$ are the incident and final photon wavevectors. The coherent states $|I\rangle$ and $|F\rangle$ are eigenvectors of the photon annihilation operators with complex eigenvalues α_I and α_F and average occupation numbers $n_I = |\alpha_I|^2$ and $n_F = |\alpha_F|^2$. One recovers the standard condition when $n_I \to 0$ so that the usual treatment is meaningful. The scattering cross-section becomes proportional to n_F and a final coherent state is expected when n_I is large and the number of final channels is small. A coherent $|F\rangle$ is not expected for $d\sigma/d\Omega|_e$, which has many open final state channels, whereas for $d\sigma/d\Omega|_{ph}$, the situation is different. In the present experiment, $\lambda_0 \approx 4$ to 5 nm; hence, the accessible volume in the reciprocal space is a small fraction of the first BZ, and only a few phonon modes, i.e., final state channels, are involved. Furthermore, a coherent initial state is present. We have:

$$\left.\frac{d\sigma}{d\Omega}\right|_{ph} = \left.\frac{d\sigma^+}{d\Omega}\right|_{ph} + \left.\frac{d\sigma^-}{d\Omega}\right|_{ph} = \frac{k}{k_0}\left[S^+_{ph}(\boldsymbol{q})\, n^+_F + S^-_{ph}(\boldsymbol{q}) n^-_F\right],$$

where we distinguish the different channels for phonon creation ($^+$) and annihilation ($^-$). $S^+_{ph}(\boldsymbol{q})$ and $S^-_{ph}(\boldsymbol{q})$ are the phonon static structure factors, i.e., the integrals of the dynamic structure factors corresponding to n^+_F and n^-_F, respectively:

$$S^+_{ph}(\boldsymbol{q},\omega) = N_{\boldsymbol{q}j} C(\boldsymbol{q}j)(\tilde{n}_{\boldsymbol{q}j}+1)\delta(\omega-\omega_{\boldsymbol{q}j})\,\delta(\boldsymbol{k}o-\boldsymbol{k}+\boldsymbol{q})$$
$$S^-_{ph}(\boldsymbol{q},\omega) = N_{\boldsymbol{q}j} C(\boldsymbol{q}j)(\tilde{n}_{\boldsymbol{q}j})\delta(\omega+\omega_{\boldsymbol{q}j})\,\delta(\boldsymbol{k}o-\boldsymbol{k}-\boldsymbol{q}).$$

Here, $C(\boldsymbol{q}j) = \left|\boldsymbol{F}_{\boldsymbol{q}j}\cdot\boldsymbol{q}\right|^2 P(\boldsymbol{\epsilon},\boldsymbol{\epsilon}_0)/(2M\omega_{\boldsymbol{q}j})$ with M atomic mass, and $P(\boldsymbol{\epsilon},\boldsymbol{\epsilon}_0)$ accounts for the effect of the beam polarizations. $\boldsymbol{F}_{\boldsymbol{q}j}$, $\hbar\omega_{\boldsymbol{q}j}$, and $\tilde{n}_{\boldsymbol{q}j}$ are the structure factor, energy and occupation number of the phonon state of momentum $\boldsymbol{q}$ in the j-th branch. $N_{\boldsymbol{q}j}$ is the number of normal modes in the scattering volume defined by the scattering solid angle. Considering that $\omega_{\boldsymbol{q}j} \ll ck_0$, we can safely set in the following $k/k_0 = 1$. As routine, the scattering equations are derived under the assumption that the incoming beam total energy is much higher than that of the scattered beam. Two effects contribute to reducing the incoming beam intensity, namely the scattering itself and the absorption. The reduction due to the scattering is related to the contribution of all possible scattering processes and results in a rather complex equation. This contribution is not negligible when the rate $dn/dt \approx n/T_p$, T_p being the pulse duration. Therefore, in the present observation, this contribution is assumed to be small enough in order to neglect it. When these effects are included, a threshold for the exponential growth could be present.

Finally, the scattered photon rate, $dn/dt = dn^+/dt + dn^-/dt$, is evaluated considering a time-dependent incident intensity, proportional to the measured I_0 through an unknown efficiency K_0, $n_0 f(t) = K_0\, I_0 f(t)$, with $\int_{-\infty}^{+\infty} f(t)dt = 1$:

$$\begin{cases} \dfrac{dn^+(t)}{dt} = n_0 f(t)\, N_{\boldsymbol{q}j}\, C(\boldsymbol{q}j)[\tilde{n}_{\boldsymbol{q}j}+1]n^+(t) \\ \dfrac{dn^-(t)}{dt} = n_0 f(t)\, N_{\boldsymbol{q}j}\, C(\boldsymbol{q}j)\tilde{n}_{\boldsymbol{q}j}(t)n^-(t), \end{cases} \quad [1]$$

where $\tilde{n}_{\boldsymbol{q}j}(t) = \tilde{n}_B(\hbar\omega_{\boldsymbol{q}j}) + n^+(t) - n^-(t)$ is the time-dependent occupation number of the $\boldsymbol{q}j$ phonon mode and $\tilde{n}_B(\hbar\omega_{\boldsymbol{q}j})$ is its Bose occupation number. In Eq. **1**, it is not specified that the quantum numbers associated with creation and annihilation have wavenumbers that are slightly different (negligibly, since $\omega_{\boldsymbol{q}j} \ll ck_0$). Both channels contribute to I_{scat}, as do all the modes within the detector solid angle.

Notice two important points: first, since QM governs the processes, the rate of phonon creation is higher than that of annihilation, $n^+(t) - n^-(t) > 0$ and, consequently, $\tilde{n}_{\boldsymbol{q}j}(t) > \tilde{n}_B(\hbar\omega_{\boldsymbol{q}j})$ and, second, the presence of $N_{\boldsymbol{q}j}$ times $C(\boldsymbol{q}j)$ will have a determining role in the exponential growth of the ratio of scattered to incident intensities. The well-known detailed balance property, at thermal equilibrium, is also a consequence of the fact that a and a^+ do not commute.

Experimental Data Fitting. In order to use the model to describe the experimental data, we recall that i) I_{scat} is measured within the collection time of the MCP detector ($t_c \approx 1$ to 2 ns) and ii) the creation and annihilation processes cannot be distinguished (the detection is energy integrated). Accordingly, we take:

$$R_{scat} = \frac{I_{scat}}{I_0} = \frac{K_0}{K}\, lim_{t\to\infty}\left[\frac{n(t)}{n_0}\right],$$

with the (unknown) proportionality constant related to the detection efficiencies K_0 and K. To model $\lim_{t\to\infty} n(t)/n_0$, we use the analytical solution for the ratio $n^+(t)/n^-(t)$, with integration constant from the system thermodynamic equilibrium state and $g(t) = \int_{-\infty}^{t} dt' f(t')$. Fixing a time $t_f > T_p$, we get:

$$\rho(t_f) = \frac{n^+(t_f)}{n^-(t_f)} = \frac{\tilde{n}_{\boldsymbol{q}j}(t_f)+1}{\tilde{n}_{\boldsymbol{q}j}(t_f)}\, \exp\left[n_0 N_{\boldsymbol{q}j} C(\boldsymbol{q}j) g(t_f)\right]. \quad [2]$$

From Eqs. **1** and **2**, we obtain the following relation, describing the exponential growth of the scattered to incoming intensity ratio. This exponential growth resembles the result of ref. 28 where, in a different context, it is found a similar behavior for the quasi-elastic scattering of light from a Bose–Einstein condensate, the common features being the small number of condensed matter states and the exponential growth.

$$\frac{n(t_f)}{n_0} \simeq C(\boldsymbol{q}j)[2\tilde{n}_B(\hbar\omega_{\boldsymbol{q}j})+1] \cdot \exp\left[\frac{1}{2} n_0 N_{\boldsymbol{q}j} C(\boldsymbol{q}j)\left(\tilde{n}_{\boldsymbol{q}j}(t_f) + \frac{\rho(t_f)}{\rho(t_f)+1}\right)\right]. \quad [3]$$

The factor $C(\boldsymbol{q}j)$ is larger for low energy longitudinal modes, and it is zero for transverse modes because the structure factor is